



Tool wear in laser ultrasonically combined turning of tungsten carbide with PCD tools

Changjuan Zhang¹ · Feng Jiao¹

Received: 4 June 2020 / Accepted: 15 October 2020 / Published online: 24 October 2020
© Springer-Verlag London Ltd., part of Springer Nature 2020

Abstract

Tungsten carbides are typical difficult-to-cut materials due to their high hardness and brittleness, which cause severe tool wear and shorten tool life when being machined during conventional processing methods, leading to a loss of quality and accuracy of the machined parts. In this paper, a novel laser ultrasonically assisted turning technology for tungsten carbides was proposed, and the primary objective of this study was to investigate the behavior of polycrystalline diamond (PCD) tools when turning tungsten carbides with the application of ultrasonic vibration to tools and laser-induced heating to workpieces. To determine suitable parameters, thermal modeling of laser ultrasonically assisted turning of tungsten carbide was employed. Through contrast experiments carried out during conventional turning, ultrasonically elliptical vibration turning, laser-assisted turning, and laser ultrasonically combined turning of tungsten carbides with PCD tools, the tool wear characteristics and dominant wear mechanisms were investigated, and the relation between tool wear and surface quality of workpiece was determined by analyzing the effects of tool wear on the surface roughness values and the microtopography of the machined surface. A significant reduction in the cutting force and a substantial improvement in the tool life were obtained in laser ultrasonically combined turning of tungsten carbides with PCD tools when compared with conventional turning, ultrasonically elliptical vibration turning, and laser-assisted turning; therefore, lower surface roughness values and a good surface quality of the workpiece were obtained. During laser ultrasonically combined turning of tungsten carbides with PCD tools, the wear on the rake face was characterized by micro tipping and chipping, the flank face had shallow micro-grooves oriented along the cutting direction, and the dominant failure mechanisms of the PCD tools were the synergistic interaction of diffusion, oxidation, tipping, and chipping. With the increase in tool wear, the surface roughness values steadily increased in laser ultrasonically combined turning, and the cutting mode was changed from ductile mode turning to brittle mode turning, which resulted in many defects, including pits, voids, grooves, etc., on the machined surfaces.

Keywords Laser ultrasonically combined turning · Tungsten carbides · PCD tools · Tool wear · Surface quality

1 Introduction

Tungsten carbides are widely used in industry as cutting and forming tools due to their excellent physical and mechanical properties, such as high hardness, superior strength, and high toughness. Moreover, their relatively high wear resistance and high chemical stability also make it more favorable compared with other counterpart materials [1, 2]. However, tungsten

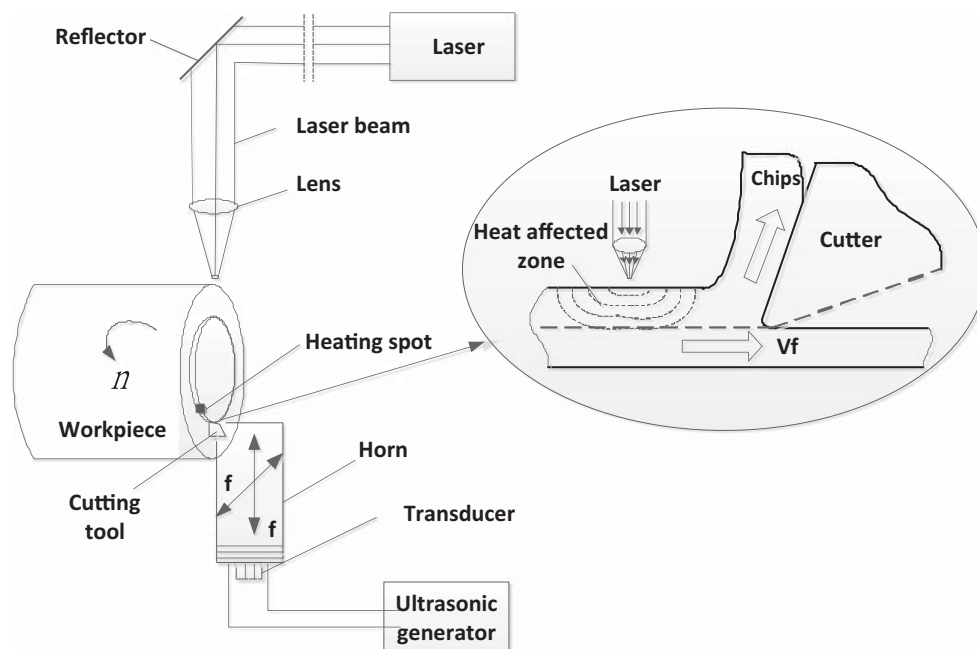
carbides are notoriously difficult to machine due to several inherent properties including high brittleness and low fracture toughness, which leads to a poor surface finish, severe cutting tool wear, and high processing cost [3]. Thus, conventional machining of tungsten carbide often indicates to be uneconomical. In addition, although the wear behavior and mechanisms of tungsten carbide used as cutting tools and mould have been widely investigated to become well known in the past decades [4–7], little work has been done on the material removal characteristics of tungsten carbide as a workpiece machined by ultrahard tools, and only a few investigations have focused on the precise and efficient machining of tungsten carbides.

Laser material processing, such as laser welding, laser forming, laser drilling, and laser machining, has been studied

✉ Changjuan Zhang
zhangcj@hpu.edu.cn

¹ School of Mechanical and Power Engineering, Henan Polytechnic University, Jiaozuo, Henan, China

Fig. 1 Schematic of LUCT



by many researchers [8–12]. Laser-assisted machining is a promising technology, in which the difficult-to-machine workpiece material is preheated to improve its machinability [13, 14]. In this process, the workpiece is subjected to a focused laser beam resulting in a localized heat flux, which significantly increases the temperature of the workpiece in the vicinity of the cutting tool; therefore, the material is thermally softened, which improves material removal and reduces cutting tool wear. According to Refs. [15–17], various types of localized and bulk heating sources were used for thermal softening of workpiece materials in hot machining. Laser-assisted machining has been successfully applied to precision cutting difficult-to-machine materials due to its superior performance such as flexible control, accurate emission, and ability to adjust the laser spot size and shape. Bejjania et al. [18] investigated the tool wear characteristics in laser-assisted turning of titanium metal matrix composites and

found that laser-assisted machining could increase the tool life by up to 180%. Anderson et al. [19] evaluated the machinability of Inconel 718 under conventional machining and laser-assisted machining with carbide and ceramic inserts. The results showed that compared with conventional machining, the surface roughness was improved 2–3-fold and the tool life increased 200–300% in laser-assisted machining.

However, the heat stress generated in the process of laser-assisted machining causes microcracks in the workpiece surface, which reduce the surface quality and increase the processing cost [20, 21]. And ultrasonically elliptical assisted machining can offer a significant improvement in the machining of difficult-to-machine materials by reducing the cutting force and cutting temperature, extending the lifetime of the cutting tool and improving the surface quality of the workpiece [22, 23]. Therefore, both ultrasonically elliptical vibration machining and laser-assisted

Table 1 Material properties of tungsten carbide

| Parameters | Value before processing | Value after processing |
|---|-------------------------|------------------------|
| Co contents (%) | 20 | 20 |
| WC contents (%) | 80 | 80 |
| Hardness (HRA) | 83 | 76 |
| Bending strength (N mm^{-2}) | 2480 | 2168 |
| Impact strength (J cm^{-2}) | 9.2 | 12.28 |
| Elasticity modulus (GPa) | 459 | 448 |
| Expansion (10^{-6} K^{-1}) | 5.8 | 7.3 |
| Thermal conductivity ($\text{W m}^{-1} \text{ K}^{-1}$) | 95 | 79 |
| Specific heat ($\text{KJ kg}^{-1} \text{ K}^{-1}$) | 250 | 272 |
| Poisson's ratio | 0.25 | 0.31 |

Table 2 Cutting tool parameters

| Parameters | Value |
|-----------------------|-------|
| Rake angle (°) | 0 |
| Clearance angle (°) | 7 |
| Inclination angle (°) | 0 |
| Edge angle (°) | 62.5 |
| Nose radius (mm) | 0.4 |
| Nose angle (°) | 55 |

machining were combined to develop a novel hybrid machining technique called laser ultrasonically combined machining. Figure 1 shows a schematic of laser ultrasonically combined face turning of a cylindrical workpiece. The workpiece performs rotary movement, and the cutting tool performs feed movement along the radial direction with speeds of v_r and v_f . The high power laser beam is focused on the workpiece surface in front of the tool edge, and the local surface is heated to a high temperature in a short period of time, which changes the material machinability at high temperature and softens the workpiece material. Moreover, the cutting tool exerts ultrasonic vibration with the same frequency in tangential and radial directions; thus, ultrasonically elliptical

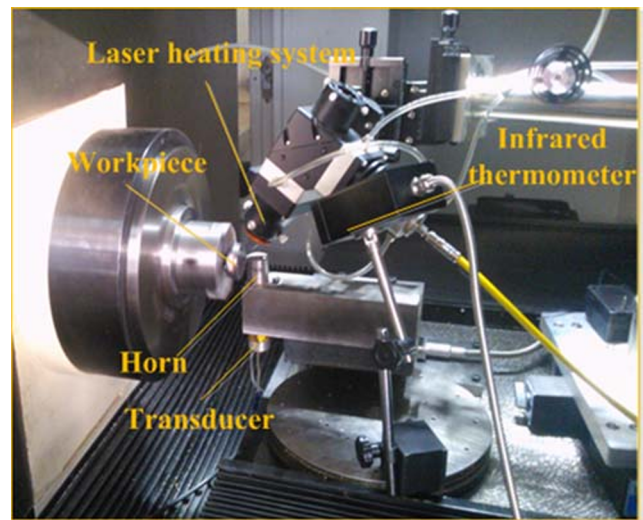
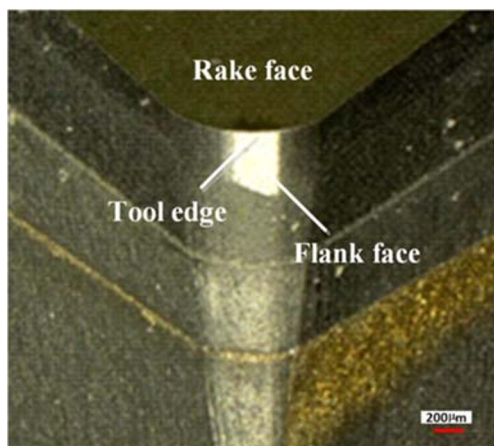
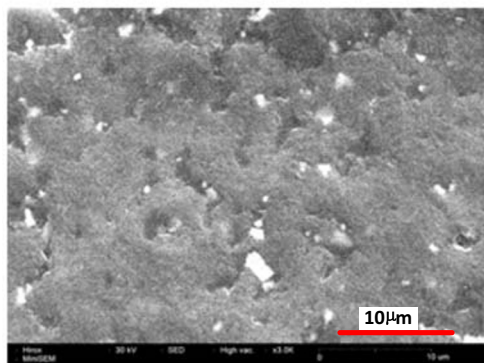


Fig. 3 LUCT experimental set-up

vibration turning of the softened workpiece is realized, which avoids the long friction between the tool flank face and the machined workpiece surface, and breakage of the cutting tool and its negative impact on the workpiece surface quality are reduced. Therefore, the tool wear can be reduced, and the surface quality of the workpiece can be improved by combining the advantages of laser-assisted cutting and ultrasonically elliptical vibration cutting techniques when used in combination with each other. Hsu et al. [24] investigated the machining characteristics of Inconel 718 by using ultrasonic and high-temperature-aided cutting. They found that when aided by ultrasonic vibration in the tangential direction, the surface roughness of the workpiece and the cutting force were reduced and the service life of the cutter was extended. Muhammad et al. [25–27] experimentally and numerically studied the hot ultrasonically assisted turning of Ti alloy and demonstrated the benefits in terms of reduction in the cutting forces and improvement in the surface roughness.



a



b

Fig. 2 Cutting tool. **a** PCD tool profile. **b** Micromorphology of the PCD tool

Table 3 Cutting parameters

| Parameters | Value |
|---|-------|
| Cutting speed ($m\ min^{-1}$) | 30 |
| Depth of cut (μm) | 15 |
| Feed rate ($mm\ rev^{-1}$) | 0.014 |
| Laser wavelength (μm) | 1.06 |
| Laser spot diameter (mm) | 0.4 |
| Laser incident angle (°) | 60 |
| Laser power (W) | 350 |
| Distance from laser spot and tool nose (mm) | 1.8 |
| Ultrasonic vibration frequency (kHz) | 35 |
| Ultrasonic tangential amplitude (μm) | 1.4 |
| Ultrasonic axial amplitude (μm) | 2.1 |

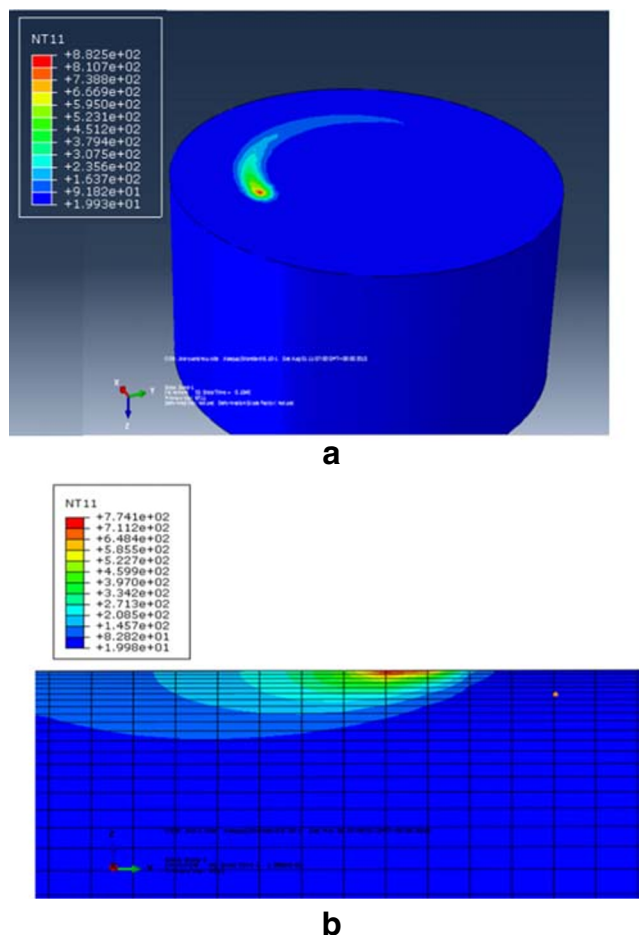


Fig. 4 Temperature distributions of the workpiece. **a** On the surface. **b** In the vertical section

Although tremendous studies involving cutting force and surface quality have been published in hot ultrasonically assisted machining difficult-to-machine materials, investigations of tool wear in laser ultrasonically combined machining of tungsten carbide work materials have not been reported. In addition, the tool wear is very severe and complex in laser ultrasonically combined cutting of tungsten carbides, and slight tool wear would cause large machining errors in the workpiece, which would greatly affect the processing efficiency and machining cost [28]. Therefore, the study of the tool wear characteristics in laser ultrasonically combined machining of tungsten carbide is of significance and necessity.

In this work, laser ultrasonically combined turning (LUCT) is proposed based on ultrasonically elliptical vibration turning (UEVT) and laser-assisted turning (LAT). To determine suitable parameters, especially laser parameters, the temperature numerical simulation of the workpiece was performed. Contrast experiments of tool wear in conventional turning (CT), UEVT, LAT, and LUCT tungsten carbides with polycrystalline diamond (PCD) tools were carried out with an ultraprecision lathe, and

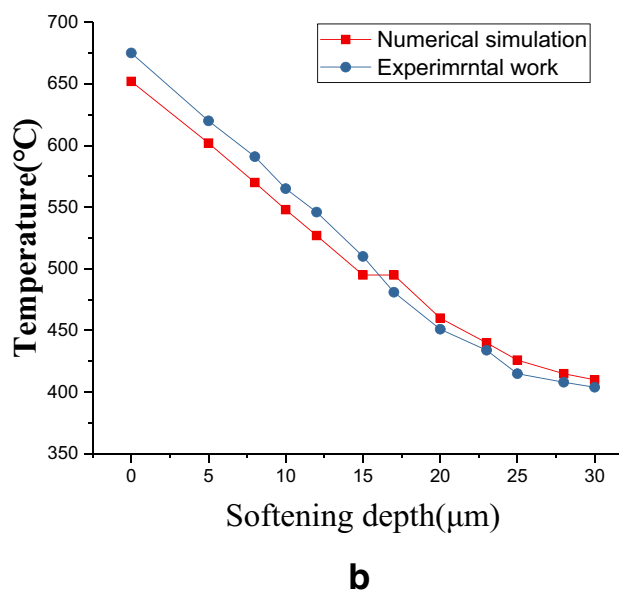
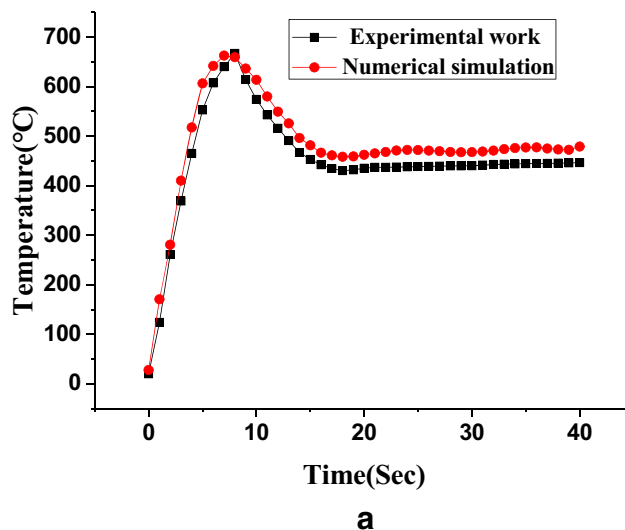


Fig. 5 Experimental and numerical temperature profiles. **a** On the surface. **b** In the vertical section

the tool wear performances and wear mechanisms were investigated during LUCT of tungsten carbides with PCD tools.

2 Experimental work

2.1 Materials of workpiece and cutting tool

In this study, a cylindrical bar of tungsten carbide with an initial diameter of 50 mm was used as the machined workpiece. The mechanical properties of tungsten carbide before and after processing are listed in Table 1. For all experiments, diamond-shaped PCD cutting tools with a side length of 7 mm were used. The shape and micrograph of the PCD tool prior to the tests are shown in Fig. 2 with the parameters given in Table 2.

2.2 Experimental setup

The LUCT experimental setup consists of ultraprecision turning system, ultrasonic vibration system, and laser heating system. As shown in Fig. 3, an ultraprecision CNC lathe, a YAG laser, an H66M ultrasonic generator, and a homebuilt ultrasonic vibration system are used during the LUCT process. The workpiece was mounted on the lathe and a tool autochecking instrument was used during the experiments to reduce the influence of tool setting errors on subsequent tool wear. In LAT experiments, the laser heating system includes laser host, laser power supply, cooling system, laser-positioning system, optical fiber transmission system, and focusing system. The laser-focusing device connected to the laser host through optical fiber was fixed on the cross slide of the lathe utilizing the bracket, and the laser spot and tool nose were kept apart a certain space by adjusting the laser position and angle. During UEVT experiments, the elliptical vibration of the tool was realized with an ultrasonic system composed of an ultrasonic generator, transducer, and horn with chutes. The ultrasonic device and a dynamometer used to record the cutting forces in real time were both fastened to the machine table, which maintained a synchronization of the ultrasonic vibration device and the laser heating system.

In the process of turning tungsten carbides, three PCD tools with the same geometric parameters were used in each of CT, UEVT, LAT, and LUCT, and the tools were retracted when feeding to 30 mm of the workpiece diameter. Then, the tool wear was determined by using a three-dimensional digital microscope (model KEYENC VHX-2000C) and scanning electron microscope (SEM). The average tool flank wear of the three cutting tools in CT, UEVT, LAT, and LUCT was obtained and the energy spectrum of the worn areas was analyzed. In addition, the cutting forces were measured using a three-component force dynamometer.

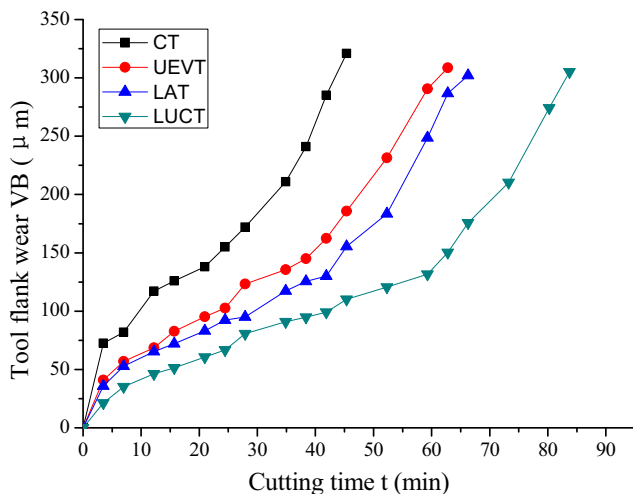


Fig. 6 Tool wear progression

2.3 Experimental parameters

Some studies have shown that the hardness of tungsten carbide was reduced drastically and the workpiece material was softened when the cutting temperature was higher than 400 °C [29, 30]. With the experimental parameters in Table 3, by using an infrared thermometer, the measured average temperature of the laser spot center on the workpiece surface and the average temperature of the cutting domain were approximately 686 °C and 425 °C, respectively. With these temperatures, the cutting performances of tungsten carbide improved and the tool life was not shortened because of the high temperature of tool nose. Therefore, the CT and UEVT experiments were carried out at room temperature, and the LAT and LUCT experiments were carried out at a cutting zone temperature of approximately 420 °C.

3 Thermal modeling of LUCT

It is necessary to precisely determine the temperature field in the workpiece undergoing laser heating to maximize the benefits of the thermal softening effects while ensuring proper heating of the workpiece in the LUCT. To study the temperature distribution in LUCT of tungsten carbide and obtain reasonable process parameters, the finite element method of ABAQUS implicit code was used in the thermal analysis of LUCT. The surface heat flux distribution is defined as

$$q_a = \frac{2\eta P}{\pi r_b^2} \text{EXP}\left(-2 \frac{r^2}{r_b^2}\right) \tag{1}$$

where P is the laser power, η is the absorption coefficient of the irradiated surface and is approximately 0.32 in this research, r_b is the effective radius of the laser, and r is the distance of a point away from the center of the laser.

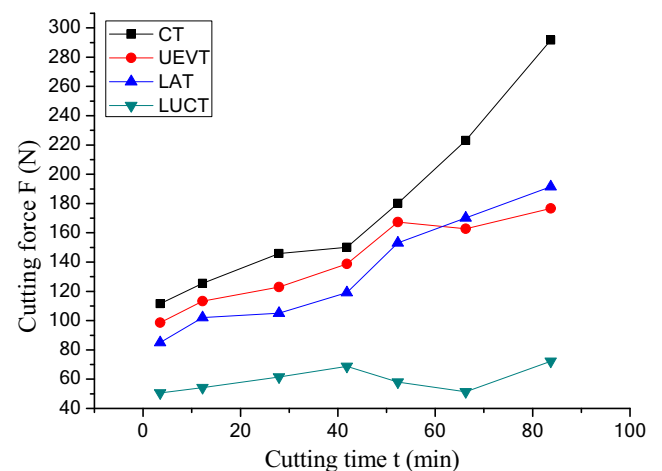
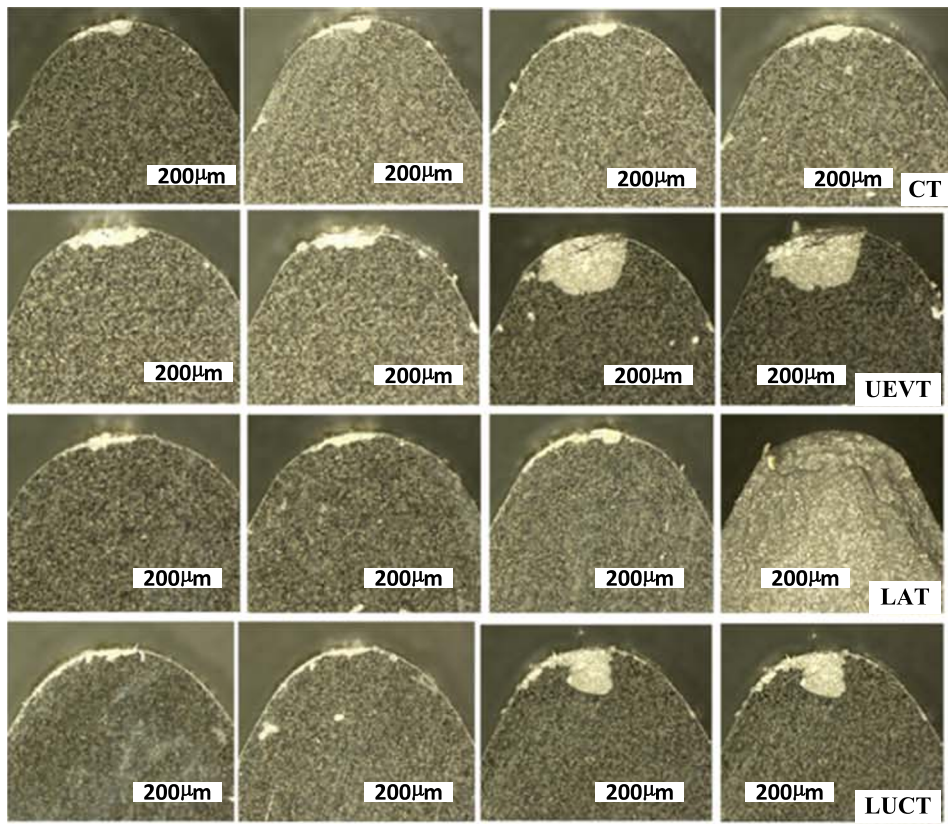
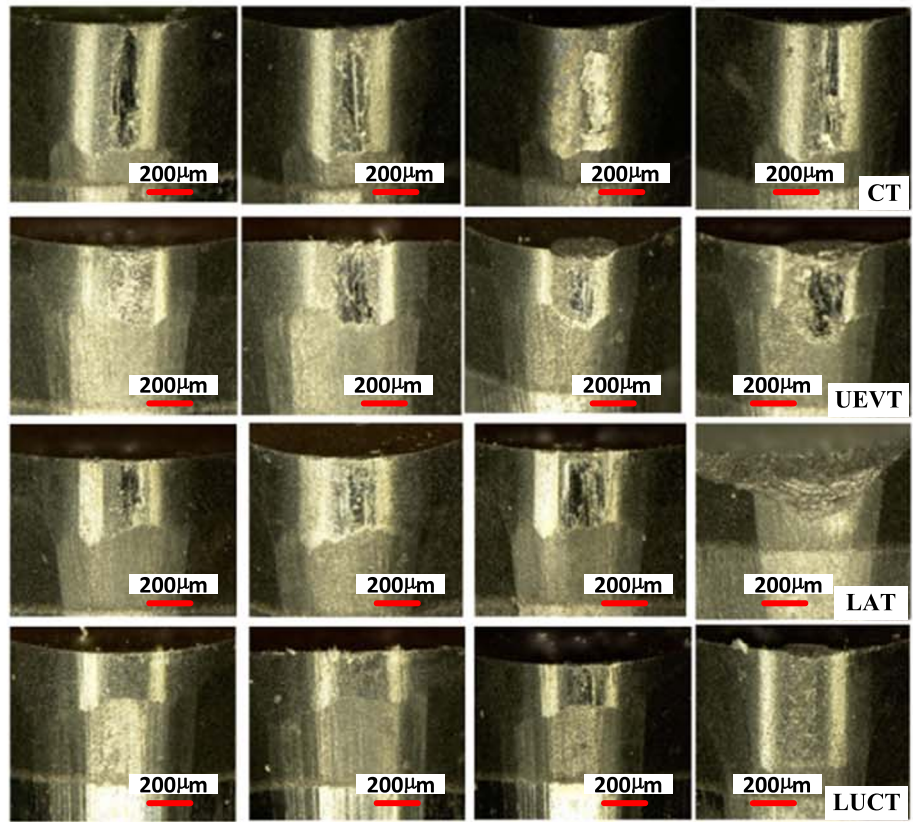


Fig. 7 Effect of tool wear on cutting force



a



b

◀ **Fig. 8** Tool wear morphologies at different tool wear times of 3.49, 15.708, 45.345, and 66.285 min from left to right. **a** Rake face. **b** Flank face

The conduction follows Fourier's law, and the heat loss rate per unit area in W m^{-2} due to conduction is

$$q_d = k \frac{\partial T}{\partial n} \quad (2)$$

where $\frac{\partial T}{\partial n}$ is the temperature gradient in the normal direction and k is the thermal conductivity. The convection follows Newton's law, and the heat loss rate per unit area in W m^{-2} due to convection is

$$q_c = h_c(T_s - T_a) \quad (3)$$

where h_c is the coefficient of convection heat transfer, T_s is the temperature of the irradiated surface, and T_a is the ambient temperature. In the LUCT of cemented carbides, the surrounding air flow is very slow and the coefficient of convection heat transfer is very small, so thermal convection can be ignored. The heat loss rate per unit area in W m^{-2} due to radiation is

$$q_r = 5.67 \times 10^{-8} \varepsilon (T_s^4 - T_a^4) \quad (4)$$

where ε is the surface emissivity, whose value depends on the surface conditions and the temperature of the workpiece. A constant surface emissivity of $\varepsilon = 0.35$ is used for the estimation of heat loss due to radiation.

In the thermal analysis, an eight-node element, DC3D8, was used. Local seeds were used to control the grid density with a minimum node size of 0.01 mm. For all simulations, dense meshes were used near the heat source to obtain more accurate results and coarse meshes were used far from the heat source to reduce the run time. Figure 4 shows the predicted temperature fields on the surface and in the vertical section of the workpiece in the LUCT of tungsten carbides. In Fig. 4b, the relationship between temperature and softening depth can be obtained, which helps to choose a suitable cutting depth.

Additionally, to evaluate the true laser-induced heat flux, the laser power, laser spot diameter, laser incident angle, and scan velocity were adjusted as 350 W, 0.4 mm, 60° , and 0.5 mm s^{-1} , respectively. The temperature of the top surface and vertical section of the workpiece were measured using an infrared thermometer. By comparing with the finite element simulations, the corresponding heat flux distribution and the temperature profile by adjustment of the heat flux parameters (laser absorption coefficient, coefficient of convection heat transfer, and surface emissivity) were obtained. Figure 5 shows the predicted temperature profiles of the numerical simulations and the experimental measurements. As shown in this figure, good agreement between the experimental and numerical measurements was obtained and the thermophysical

parameters of the materials and the heat flux parameters in the simulation reflected the actual experimental conditions, which validated the accuracy of the thermal model and provided guidance for selecting appropriate laser parameters in the LUCT of tungsten carbides.

4 Results and analysis

4.1 Tool life

To understand the effects of ultrasonic vibration and laser heating on improving the tool life, tool wear progression was analyzed as shown in Fig. 6. It was found that there were three worn stages, an initial worn stage, a normal worn stage, and an acute worn stage in CT, UEVT, LAT, and LUCT, but the node of each wear stage and the tool life were different. Compared with the other three cutting modes, in LUCT, the smallest tool flank wear could be obtained, the tool wear speed reduced significantly, and the increase in tool life was 95.3%, 34.96%, and 25.76%, respectively. Moreover, a substantial reduction of the flank wear was observed in CT, UEVT, LAT, and LUCT with the same cutting time, and as the cutting time increased, the flank wear under each cutting mode also increased, but the wear rate during each stage was different. During the initial worn stage, there were few differences in the wear rate among CT, UEVT, LAT, and LUCT because of the sharpness and good thermal conductivity of the PCD tool and the smaller cutting force. During the normal worn stage, the wear rates in the UEVT and LAT were basically the same, and in the LUCT, the cutting time was longer during the normal worn stage. During the acute worn stage, the cutting forces in CT and LAT significantly increased, which caused the wear rates to increase rapidly and even led to breakage of the cutting tool. A significant reduction by 24.6% and 20% in the average thrust force was observed with the application of ultrasonic vibration to the cutting tool and thermal softening to the workpiece material in UEVT and LAT, respectively, as shown in Fig. 7, resulting in the smaller difference and its significant reduction in PCD tool flank wear when compared with CT. During LUCT, with the advantages of ultrasonic vibration and laser heating, a significant reduction by 67.5% in the average thrust force compared with that in CT caused a dramatic reduction in the PCD tool flank wear and wear rate.

4.2 Tool wear characteristics

The digital microscope images of the PCD tool wear on the rake face and flank face when the cutting time increased gradually in CT, UEVT, LAT, and LUCT tungsten carbides are shown in Fig. 8. It was found that during the initial and normal worn stages, peeling of the PCD tool was generated near the tool edge on the rake face, especially in UEVT, and sheet

delamination occurred due to the high-frequency intermittent impact. In CT, UEVT, and LAT, the flank wear region of the PCD tool was covered with obvious micro-grooves oriented along the cutting direction, especially in LAT. The depth of the micro-groove in the flank wear region increased notably after cutting for 90.69 min, and tool breakage occurred as the cutting time increased to 132.57 min, which was mainly attributed to the abrasion, diffusion, and oxidation wear of the cutting tool generated by the cutting force, and to the temperature which reduced the strength and hardness of the cutting tool, resulting in repeated scratching of the workpiece on the tool flank face. In addition, serious wear of the PCD tool could be observed during the acute wear stage in LUCT because the high hardness of the workpiece material magnified the contact pressure and friction between the workpiece and the tool edge and the actual rake angle of the tool changed from zero to positive, with the complex alternating stress and the vibration impact between the tool and workpiece in the process of reciprocating vibration causing the chipping and tipping of the PCD tool.

4.3 Tool wear mechanism

Figure 9 shows the worn surfaces of the PCD tools in CT, UEVT, LAT, and LUCT of tungsten carbides. The cutting tool showed peeling, tipping, and chipping wear during tungsten carbide turning, with and without ultrasonic vibration and laser heating. Moreover, evidence of adhesion of the workpiece material can be found, especially in the process of CT

and LAT of tungsten carbides. The high cutting force and temperature at the chip-tool interface can promote adhesion on the tool rake and flank face, as indicated by the plastic flow of the workpiece material, and a continuous layer of adhered workpiece material was apparent on the flank face. These material pieces, which adhere unsteadily, get worn off and carry away material adhered through bonds weakened by the thermally activated processes in the surface layer of the PCD tools; as a result, the diamond particles near the tool edge are removed due to the instability in the chip formation, high cutting force, and oscillations in the cutting process, which result in the tipping and chipping of PCD tools during the machining of tungsten carbides [31]. In addition, Fig. 10 shows the chemical composition of zones A and B in the flank wear area shown in Fig. 9 during CT and LAT of tungsten carbides with PCD tools. The C elements not being detected on the tool flank face indicated that the detected zone was covered with the workpiece material and that adhesion wear of PCD tools occurred.

Table 4 lists the element composition of the tool nose when CT, UEVT, LAT, and LUCT of tungsten carbides. The presence of W elements, which are not part of the PCD material, and evidence of diffusion of other elements into the PCD tool and vice versa (Co, Ni, and Si), especially in LAT and LUCT, reduced the inertia of PCD and increased the affinity of PCD to alloy constituents. When the cutting force and temperature among the tool, chip, and workpiece reached a certain value, adhesion wear of the tools was generated, and the increase in Ni elements further enhanced the adhesion strength

Fig. 9 SEM micrographs of the cutting tools

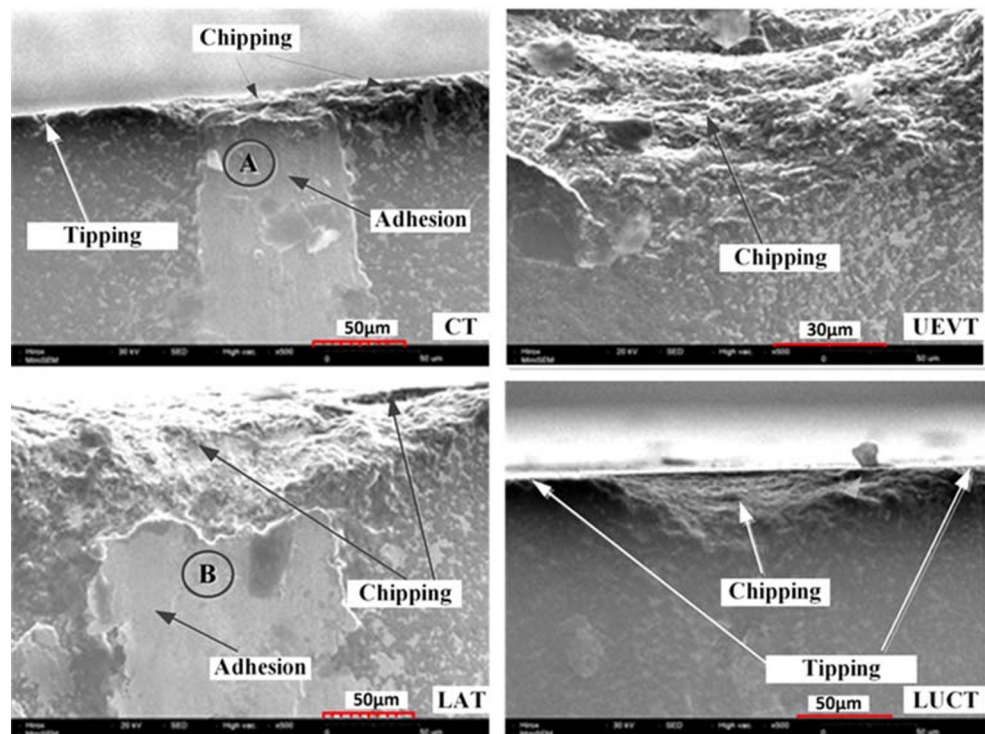
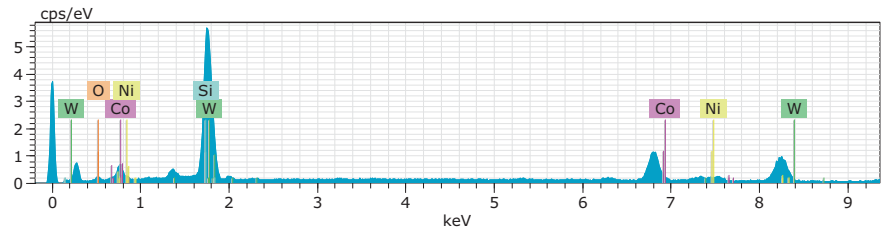
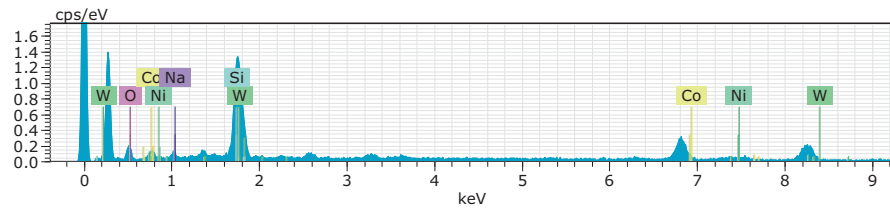


Fig. 10 EDS energy spectrum of the adhered layer in CT and LAT



CT

| El | AN | Series | unn. [wt.%] | C norm. [wt.%] | C Atom. [at.%] | C Error (1 Sigma) [wt.%] |
|--------|----|----------|-------------|----------------|----------------|--------------------------|
| W | 74 | L-series | 17.68 | 45.93 | 13.04 | 0.58 |
| Si | 14 | K-series | 10.89 | 28.29 | 52.56 | 0.50 |
| Co | 27 | K-series | 4.75 | 12.34 | 10.92 | 0.18 |
| Ni | 28 | K-series | 3.30 | 8.58 | 7.63 | 0.14 |
| O | 8 | K-series | 1.87 | 4.86 | 15.86 | 0.50 |
| Total: | | | 38.50 | 100.00 | 100.00 | |



LAT

| El | AN | Series | unn. [wt.%] | C norm. [wt.%] | C Atom. [at.%] | C Error (1 Sigma) [wt.%] |
|--------|----|----------|-------------|----------------|----------------|--------------------------|
| W | 74 | L-series | 11.63 | 37.92 | 8.01 | 0.53 |
| Si | 14 | K-series | 7.03 | 22.91 | 31.66 | 0.36 |
| O | 8 | K-series | 5.37 | 17.52 | 42.49 | 1.39 |
| Co | 27 | K-series | 4.33 | 14.12 | 9.30 | 0.22 |
| Ni | 28 | K-series | 1.24 | 4.05 | 2.68 | 0.10 |
| Na | 11 | K-series | 1.07 | 3.48 | 5.87 | 0.14 |
| Total: | | | 30.68 | 100.00 | 100.00 | |

and promoted adhesion wear, resulting in tipping and chipping of the tool edge and graphitization of the diamond particles. Therefore, during LAT of tungsten carbides with PCD tools, diffusion into the workpiece accelerates the graphitizing process of the PCD tool because of the high

Table 4 Chemical composition of the tool nose worn zone

| Cutting modes | Atomic (%) | | | | | | |
|---------------|------------|-------|------|------|------|------|------|
| | C | W | Co | O | Si | Na | Ni |
| Virgin tool | 90.3 | | 6.45 | | 1.28 | | 1.97 |
| CT | 65.8 | 13 | 5.28 | 3.57 | 8.21 | 0.77 | 3.36 |
| UEVT | 65.63 | 14.44 | 6.77 | 4.33 | 6.30 | 0.60 | 1.92 |
| LAT | 73.47 | 7.72 | 5.90 | 5.19 | 4.43 | 1.25 | 2.06 |
| LUCT | 82.59 | 4.03 | 1.63 | 7.60 | 1.30 | | 1.34 |

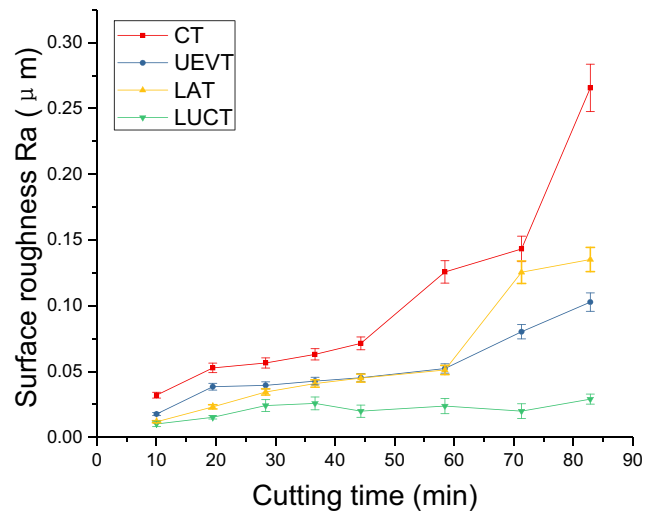


Fig. 11 Effect of tool wear on surface roughness

Fig. 12 Surface morphology of the machined workpiece

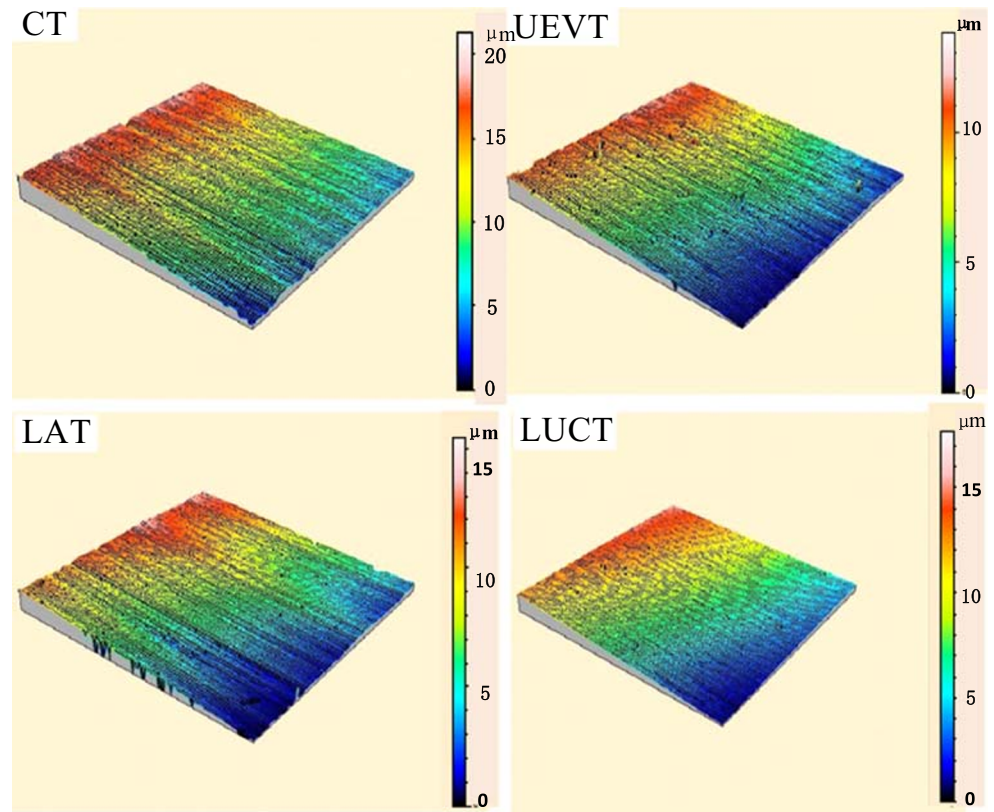
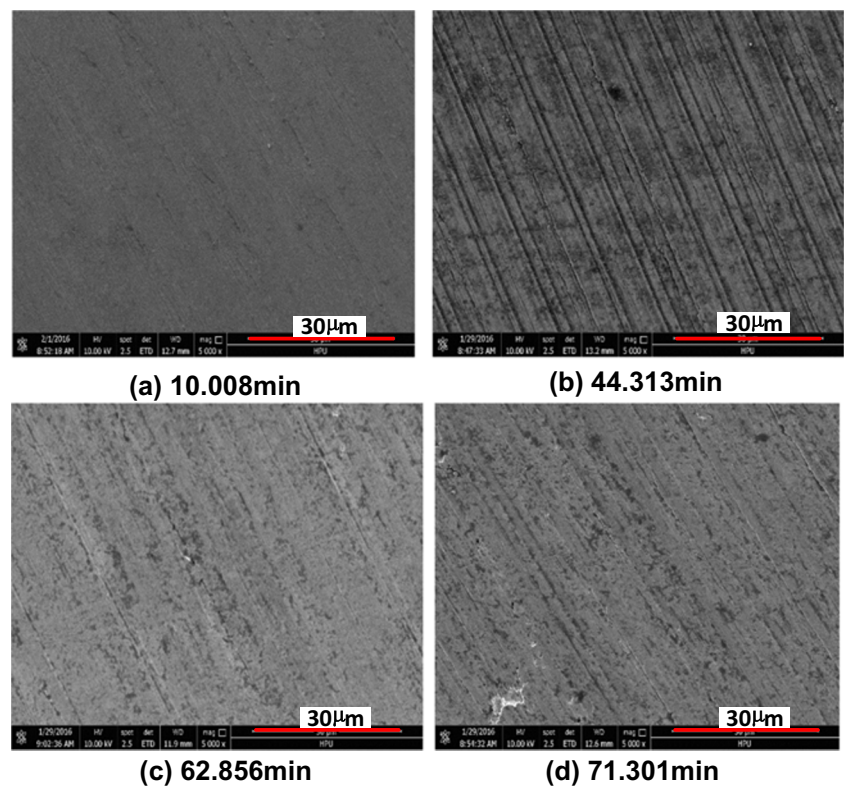


Fig. 13 SEM micrographs of the machined surface in LUCT. **a** 10.008 min. **b** 44.313 min. **c** 62.856 min. **d** 71.301 min



compressive stress and high cutting temperature, which promoted the PCD tool wear and reduced the tool life.

In addition, the increase in O elements in Table 4 shows evidence of oxidation wear in the event of graphitization during the turning of tungsten carbides with PCD tools, especially in LAT and LUCT. At a high cutting temperature, the Co elements can react chemically with the O elements, and the C elements are replaced, decreasing the strength of the PCD tool and resulting in the removal of the diamond particles, thereby promoting PCD tool wear. Moreover, oxidation also causes the formation of an oxide film extruded and rubbed continuously by the chip and workpiece on the edge of the tool wear zone, which promotes tool wear.

5 Effects of tool wear on surface quality

During tungsten carbide turning with PCD tools, an optical fiber white interferometer (CCI600) and SEM (Quanta 250FEG) were used to examine the roughness and microtopography of the machined surfaces. The degree of tool wear has a direct effect on the surface roughness produced in the cutting process. The Ra surface roughness values of the workpiece as a function of the tool wear times are shown in Fig. 11.

The surface roughness values in CT, UEVT, LAT, and LUCT increased with increasing cutting time, which was consistent with the trend observed in the cutting force and tool flank wear curves, and better surface roughness values were obtained in LUCT. When compared with CT, UEVT, and LAT, a significant reduction in the surface roughness by 79%, 60%, and 64%, respectively, was observed in LUCT. A small increase in the surface roughness values was found before the cutting time reached 44 min in CT and 58 min in UEVT and LAT, which indicated that a higher surface quality of the workpiece could be obtained when the tool was in a stable normal wear stage; subsequently, the surface roughness values increased dramatically. As the cutting time reached 82 min, when compared with the minimum in CT, UEVT, and LAT, the surface roughness values of the workpiece increased 7, 4.5, and 10 times, respectively, which showed that the PCD tools underwent unstable acute wear and the surface quality of the workpiece decreased. However, during LUCT of tungsten carbides with PCD tools, taking advantage of the laser-induced softening of the workpiece material and ultrasonic intermittent vibration machining, the material performance of the workpiece improved and the cutting force and tool wear decreased, resulting in a surface roughness value of the workpiece of $0.029 \mu\text{m}$ when the cutting time was 82 min, and increased by less than 2 times of the minimum surface roughness value. At this time, the PCD tool was still in a normal wear stage, and a higher surface quality of the workpiece could still be obtained.

The workpiece surface topographies in CT, UEVT, LAT, and LUCT are shown in Fig. 12. Deep micro grooves on the machined surface with obvious brittleness removal characteristics were found in CT; however, the grooves were narrower and shallower, and micro plastic deformation was observed in UEVT. In LAT and LUCT, notable plastic deformation occurred, and the micro grooves mostly disappeared; especially in LUCT, good surface quality was obtained, and the machined surface was smoother.

Figure 13 shows the microtopography of the machined surface of tungsten carbide with different cutting times in LUCT. The workpiece surfaces showed many defects, including pits, voids, and grooves (scratches), and these defects had an intimate effect on the process of tool wear. As shown in Fig. 13a, cutting occurred through a ductile mode, and the workpiece surface was very smooth in the beginning of the LUCT. The micro topography of the workpiece surface after a cutting time of 44.313 min is shown in Fig. 13b. The removal method of tungsten carbide still mostly occurred through a ductile removal mode, but many obvious grooves plowed on the workpiece surface in response to the applied cutting force and increased temperature on the machined surface. In addition, material swelling occurred and was obvious from the plastic side flow of the matrix, which remained on the cutting edge and was subjected to sufficiently high pressure causing the matrix to flow to the side of the active cutting edge [32]. Moreover, the cutting force along the main cutting edge of the tool pushed the workpiece material towards the tool nose, causing it to flow to the free surface. In Fig. 13c, some defects appeared on the workpiece surface after a cutting time of 62.856 min, and the workpiece material began to be brittle removed. With high cutting force and temperature, the severe tool wear and vibration impact result in some particles being pulled out of the machined surface; therefore, many pits and voids were left in the surface. Moreover, during the course of some particles being pulled out or crushed, the matrix around them might also be broken up. When the cutting time reached 71.301 min, the workpiece surface breakage accelerated, and the material was completely brittle, which dominated the material removal mode, as shown in Fig. 13d.

6 Conclusions

In this work, a new hybrid machining process called laser ultrasonically combined turning (LUCT) is proposed. The temperature numerical simulation of the workpiece and experimental verification were performed. And the PCD tool wear and its effect on the machined surface of a workpiece of tungsten carbides were experimentally evaluated and compared with three other techniques, including conventional turning (CT), ultrasonically elliptical vibration turning (UEVT) and laser-assisted turning (LAT). The following can be concluded:

1. Good agreement between the experimental and numerical results of temperature distribution of the workpiece was obtained; the accuracy of the thermal model was validated, which provided guidance for selecting appropriate laser parameters in the LUCT of tungsten carbides.
2. When compared with CT, UEVT, and LUCT, a significant reduction in cutting forces by 67.5%, 24.6%, and 20%, respectively, can be observed in LUCT, and a substantial improvement in the tool life by 95.3%, 34.96%, and 25.76%, respectively, can be obtained in LUCT of tungsten carbides with PCD tools.
3. The wear of the rake and flank faces are the dominant failure modes when turning tungsten carbides with PCD tools. The tool wear on the rake face is characterized by micro tipping and chipping during the later stage in LUCT; the flank face shows micro-grooves oriented along the cutting direction, and the grooves are narrower and shallower during LUCT.
4. Diffusion and oxidation are the dominant wear mechanisms in LUCT of tungsten carbides with PCD tools, and tipping and chipping are the abnormal wear patterns of PCD tools.
5. Application of ultrasonic vibration and laser heating reduces the surface roughness of the machined workpiece, and the change in the roughness values is stable in LUCT. During the process of LUCT of tungsten carbides with PCD tools, the machined surfaces show many defects of pits, voids, grooves, etc., and a poor surface quality can be observed at the end of tool wear.

Funding This work is supported by the National Natural Science Foundation of China (No. 51075127) and the Henan Research Program of Fundamental and Frontier Technology (No. 152300410102).

References

1. Konyashin I, Klyachko LI (2015) History of tungsten carbides in the Soviet Union[J]. *Int J Refract Met Hard Mater* 49:9–26
2. Mukhopadhyay A, Basu B (2011) Recent developments on WC-based bulk composites[J]. *J Mater Sci* 46(3):571–589
3. Zhan ZB, He N, Li L, Shrestha R, Liu JY, Wang SL (2015) Precision milling of tungsten carbide with micro PCD milling tool[J]. *Int J Adv Manuf Technol* 77(9-12):2095–2103
4. Hosseinkhani K, Ng E (2018) A hybrid experimental and simulation approach to evaluate the calibration of tool wear rate models in machining[J]. *Int J Adv Manuf Technol* 96(5-8):2709–2724
5. Stanciu VI, Vitry V, Delaunois F (2016) Tungsten carbide powder obtained by direct carburization of tungsten trioxide using mechanical alloying method[J]. *J Alloys Compd* 659:302–308
6. Emanuelli L, Pellizzari M, Molinari A, Castellani F, Zinutti E (2016) Thermal fatigue behaviour of WC-20Co and WC-30(CoNiCrFe) cemented carbide[J]. *Int J Refract Met Hard Mater* 60:118–124
7. Vereschaka AA, Vereschaka AS, Batako AD, Hojaev OK, Mokritskii BY (2016) Development and research of nanostructured multilayer composite coatings for tungsten-free carbides with extended area of technological applications[J]. *Int J Adv Manuf Technol* 87(9-12):3449–3457
8. Safari M, Mostaan H (2016) Experimental and numerical investigation of laser forming of cylindrical surfaces with arbitrary radius of curvature [J]. *Alex Eng J* 55(3):1941–1949
9. Safari M, Farzin M, Mostaan H (2017) A novel method for laser forming of two-step bending of a dome shaped part [J]. *Iran J Mater Form* 4(2):1–14
10. Safari M, Farzin M (2015) Experimental investigation of laser forming of a saddle shape with spiral irradiating scheme[J]. *Opt Laser Technol* 66:146–150
11. Safari M, Mostaan H, Farzin M (2016) Laser bending of tailor machined blanks: effect of start point of scan path and irradiation direction relation to step of the blank [J]. *Alex Eng J* 55(2):1587–1594
12. Safari M, Joudaki J (2018) Prediction of bending angle for laser forming of tailor machined blanks by neural network [J]. *Iran J Mater Form* 5(1):47–57
13. Song HW, Dan JQ, Chen X, Xiao JF, Xu JF (2018) Experimental investigation of machinability in laser-assisted machining of fused silica[J]. *Int J Adv Manuf Technol* 97(1-4):267–278
14. Venkatesan K, Ramanujam R, Kuppan P (2014) Laser assisted machining of difficult to cut materials: research opportunities and future directions - a comprehensive review[J]. *Procedia Eng* 97: 1626–1636
15. Hedberg GK, Shin YC, Xu L (2015) Laser-assisted milling of Ti-6Al-4V with the consideration of surface integrity[J]. *Int J Adv Manuf Technol* 79(9-12):1645–1658
16. Gao YF, Wang G, Bermingham MJ, Dargusch MS (2015) Cutting force, chip formation, and tool wear during the laser-assisted machining of a near-alpha titanium alloy BTi-6431S[J]. *Int J Adv Manuf Technol* 79(9-12):1949–1960
17. Germain G, Santo PD, Lebrun JL (2011) Comprehension of chip formation in laser assisted machining[J]. *Int J Mach Tool Manu* 51(3):230–238
18. Bejjani R, Shi B, Attia H, Balazinski M (2011) Laser assisted turning of titanium metal matrix composite[J]. *CIRP Ann Manuf Technol* 60(1):61–64
19. Anderson M, Patwa R, Shin YC (2006) Laser-assisted machining of Inconel 718 with an economic analysis[J]. *Int J Mach Tool Manu* 46(14):1879–1891
20. Zhang HZ, Kong XJ, Yang LJ, Wang Y, Chi GX (2015) High temperature deformation mechanisms and constitutive modelling for Al/SiCp/45 metal matrix composites undergoing laser-assisted machining[J]. *Mater Sci Eng A* 642:330–339
21. Kim IW, Lee CM (2016) A study on the machining characteristics of specimens with spherical shape using laser-assisted machining[J]. *Appl Therm Eng* 100:636–645
22. Zhu WL, Xing YQ, Ehmann KF, Ju BF (2016) Ultrasonic elliptical vibration texturing of the rake face of carbide cutting tools for adhesion reduction[J]. *Int J Adv Manuf Technol* 85(9-12):2669–2679
23. Chen P, Tong JL, Zhao JS, Zhang ZM, Zhao B (2020) A study of the surface microstructure and tool wear of titanium alloys after ultrasonic longitudinal-torsional milling[J]. *J Manuf Process* 53:1–11
24. Hsu CY, Lin YY, Lee WS, Lo SP (2008) Machining characteristics of Inconel 718 using ultrasonic and high temperature-aided cutting[J]. *J Mater Process Technol* 198(1-3):359–365
25. Muhammad R, Roy A, Silberschmidt VV (2013) Finite element modelling of conventional and hybrid oblique cutting processes of titanium alloy[J]. *Procedia CIRP* 8:510–515
26. Muhammad R, Maurotto A, Roy A, Silberschmidt VV (2012) Hot ultrasonically assisted cutting of β -Ti alloy[J]. *Procedia CIRP* 1: 336–341
27. Muhammad R, Maurotto A, Demiral M, Roy A, Silberschmidt VV (2014) Thermally enhanced ultrasonically assisted cutting of Ti alloy[J]. *CIRP J Manuf Sci Technol* 7(2):159–167

28. Nooraie RY, Safari M, Pak A (2020) Tool wear estimation in machining based on the flank wear inclination angle changes using the FE method [J]. *Mach Sci Technol* 24(3):425–445
29. Schenck SR, Gottschall RJ, Williams WS (1978) Deformation of cemented carbides: high temperatures, stress relaxation, and strain-rate dependence[J]. *Mater Sci Eng* 32(3):229–239
30. Buss K, Mari D (2004) High temperature deformation mechanisms in cemented carbides and cermets studied by mechanical spectroscopy[J]. *Mater Sci Eng A* 370(1-2):163–168
31. Bian R, He N, Ding WZ, Liu SQ (2017) A study on the tool wear of PCD micro end mills in ductile milling of ZrO₂ ceramics[J]. *Int J Adv Manuf Technol* 92(5-8):2197–2206
32. Ge YF, Xu JH, Yang H, Luo SB, Fu YC (2008) Workpiece surface quality when ultra-precision turning of SiCp/Al composites[J]. *J Mater Process Technol* 203(1-3):166–175

Publisher's note Springer Nature remains neutral with regard to jurisdictional claims in published maps and institutional affiliations.